Article

# Insights from Fragment Hit Binding Assays by Molecular Simulations

Noelia Ferruz,[†] Matthew J. Harvey,[‡] Jordi Mestres,[§] and Gianni De Fabritiis[*,†,‖]

[†]Computational Biophysics Laboratory (GRIB-IMIM), Universitat Pompeu Fabra, Barcelona Biomedical Research Park (PRBB), Doctor Aiguader 88, 08003 Barcelona, Barcelona, Spain

[‡]Acellera, Barcelona Biomedical Research Park (PRBB), Doctor Aiguader 88, 08003 Barcelona, Barcelona, Spain

[§]Systems Pharmacology, Research Program on Biomedical Informatics (GRIB), IMIM Hospital del Mar Medical Research Institute and Universitat Pompeu Fabra, Doctor Aiguader 88, 08003 Barcelona, Barcelona, Catalonia, Spain

[‖]Institució Catalana de Recerca i Estudis Avançats, Passeig Lluis Companys 23, 08010 Barcelona, Barcelona, Spain

Ⓢ *Supporting Information*

ABSTRACT: Novel bioactive molecules can be rationally designed by growing and linking small fragments. Because fragments are fast and promiscuous, it is common to have contradictory hit results between different experimental screening techniques. Here, we simultaneously determine fragment binding poses, affinities, and kinetics on a focused library of 42 fragments against the serine protease factor Xa using multimillisecond molecular dynamics simulations. We predict experimental poses of 12 over 15 S1 crystal structures, and affinities are recovered for 4 out of 6. A kinetic map of protein cavities is computed in terms of on- and off-rates as well as insights into secondary ligand poses. The results suggest that the approach can be useful to recapitulate discordant fragment screening data.
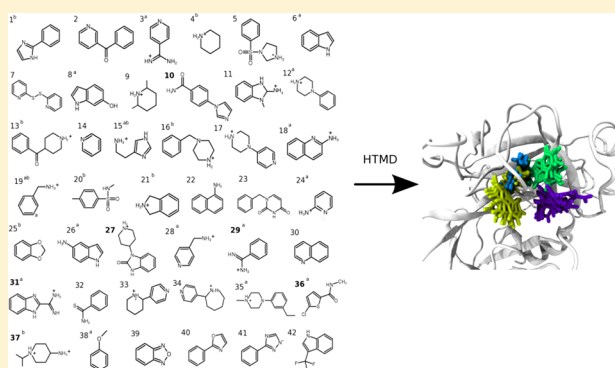
INTRODUCTION

Since scientists at Abbott laid the groundwork for the structure–activity relationship (SAR) by NMR concept in the mid-1990s,[1] fragment-based drug design (FBDD)[2] has generated several clinical drug candidates, a notable example being vemurafenib approved by the FDA in 2011.[3] The method offers several advantages[4] like efficient chemical space exploration, high ligand efficiency (LE), and stepwise growth of ligands that allows simultaneous optimization of potency and physical chemistry properties.

An early step in the FBDD process is fragment hit identification which involves characterization of the binding properties of a library of small molecule fragments against a specific target. By definition, fragments are low molecular weight entities of relatively simple structure that, while boasting high ligand efficiency (LE), usually lack potency and selectivity. These properties make characterization challenging, requiring sensitive techniques such as X-ray crystallography, surface plasmon resonance (SPR), isothermal titration calorimetry (ITC), and nuclear magnetic resonance (NMR) spectroscopy. Yet, fragment solubility and protein stability often limit the applicability of these techniques.[5] Furthermore, each different experimental assay will frequently return different fragment hits, and orthogonal validations have become widespread.[6,7] Therefore, a comprehensive fragment screening assay that can simultaneously determine the potency, kinetics, and binding poses of fragment hits would help to rationalize experimental data.

Although there have been several examples of successful computational applications in drug design,[8] in silico FBDD's impact on lead development has been limited to date. Inability to describe kinetics and conformational changes upon binding are some of the reasons.[9,10] Here, we performed a comprehensive computational assay for fragment hit characterization, for which we produced and analyzed 2.1 ms of unbiased all-atom high-throughput molecular dynamics (HTMD) data.[11,12] Our results show good agreement with available experimental data and offer an insight into the protein's binding characteristics. The entire set of filtered trajectories and a template analysis script can be obtained upon request to the authors.

The use of molecular simulations to obtain a more accurate description of binding has been already used to predict protein pharmacophores with high concentration simulations of simple chemical groups and by measuring affinity by occupancy counting.[13,14] These approaches, however, require the simulations to be in the equilibrium regime, and therefore it is possible only for extremely simple and fast chemical groups way smaller than any fragment library. Even if the equilibrium-sampling requirement was not totally met in practice for such tiny ligands, the method has shown to be better than other predictor in pharmacophore prediction.[15] Here, we rather use a new approach consisting of many out-of-equilibrium unbiased

simulations where only transitions between regions in local equilibrium are necessary. A Markov state model analysis is later used to reconstruct the full equilibrium behavior. This approach was able to substantially overcome the limitation of equilibrium simulations for folding.[16−18] In 2011 we started to apply it for binding of benzamidine to Trypsin.[19] It is also amenable to more clever adaptive sampling schemes.[20,21] This study with 42 ligands represents the largest application of the methodology to-date with any other limited to less than ten and often just one ligand.[12,21−23] We note that the final aim is to reach simulations of a full fragment library of 1000 ligands.

For this study we selected human factor Xa, a well-characterized globular protein target with extensive experimental data. Factor Xa is a trypsin-like serine protease that converts prothrombin to active thrombin playing a key role in blood coagulation. As such, the protein has been an attractive target for anticoagulant agents, and there is a wealth of structural and thermodynamic data. Factor Xa consists of a heavy and a light chain held together by a disulfide bond. The protein active site is located on the heavy chain and contains 4 subpockets, defined as S1, S2, S3, and S4, but only pockets S1 and S4 are typically exploited by anticoagulants (Figure 1). The
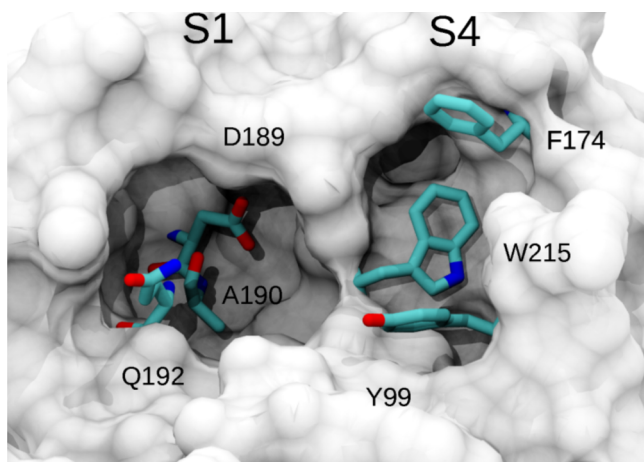

Figure 1. Overview of the protein's active site. The S1 and S4 pockets are the specific cavities exploited by factor Xa inhibitors. The S1 pocket is defined by D189, A190, and Q192 and favors positively charged moieties and aryl halogens. The S4 pocket is formed by the aromatic residues Y99, F174, and W215 and favors both hydrophobic and basic moieties. The two pockets are separated by a loop containing residues 215 to 225.

S1 pocket is a narrow cavity which favors positively charged moieties and aryl halogens,[24] whereas the S4 pocket is a shallow groove which favors aromatic, hydrophobic, and basic moieties.[25] PDB structure 1FAX[26] was used in this work.

The fragment library used herein was specifically designed to include fragments from previous NMR[27] and X-ray screenings, moieties known to bind S1 and S4 pockets, and in-house designed fragments likely to exhibit affinity. In detail, the final focused library contained 42 compounds, divided into four overlapping sets (Figure 2). The first set comprises the six fragments for which there are available thermodynamic data (in bold). The second set is comprised by 15 fragments, which have shown experimental evidence of being an S1 binder (superscript a), whereas the third set comprises ten fragments characterized as S4 binders (superscript b). Of these, fragments 15 and 19 are expected to bind either subpocket, as they have
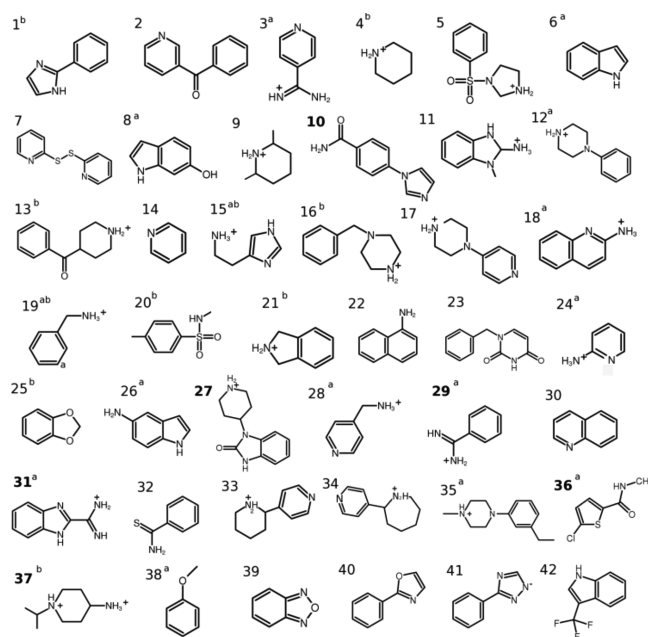

Figure 2. Fragment library. The fragment library used for the study in the simulated protonation states. The library was specifically assembled to include fragments with available thermodynamic data (in bold) and experimentally well-characterized as S1 (a superscript) and S4 moieties (b superscript).

both been crystallized in the S1 pocket of trypsin and are also present as moieties in S4 in X-ray structures of factor Xa inhibitors.[28,29] Fragment 29 (benzamidine) has been used as a control in many screenings, and its thermodynamic, kinetic, and crystallographic data is well characterized in the literature. The fourth set is comprised of fragments 1−34 that were part of a previous NMR screening.[27] Nine of them showed sub-mM affinity, of which four were reported (10, 27, 29, 31). Fragments 39−42 were manually designed for this study. The experimental references for each fragment are shown in Table S1.

RESULTS

The complete energetic and kinetic information on the 42 fragments is presented as an html table in the Supporting Information. For each fragment a total time of 45 to 100 μs of trajectory data was obtained by performing free diffusion[19] all-atom molecular dynamics simulations with the ACEMD[30] molecular dynamics software on the distributed computing project GPUGRID.[31] These data was analyzed using the HTMD software,[32] which uses a Markov state modeling (MSM)[19] method able to produce quantitative estimations of k_{on}, k_{off}, and ΔG^0 for multiple binding poses on the protein surface (Supporting Information, **Methods**).

The MSM analyses have been successfully used in a wide range of problems from ligand binding[17,19,33] to the characterization of protein folding[34] and intrinsically disordered protein dynamics.[35] For example, fragment 31's binding poses, its free energies, and first-mean passage times are shown in Figure 3. Four different free-energy minima are found, corresponding to the unbound state (1), 2 metastable states (2 and 3), and the bound state (4). The stationary distribution predicts that the bound pose is mostly populated in equilibrium (99.5% ± 0.3%), whereas all other states are only minimally occupied (populations below 0.5%). One can compute the Gibbs free
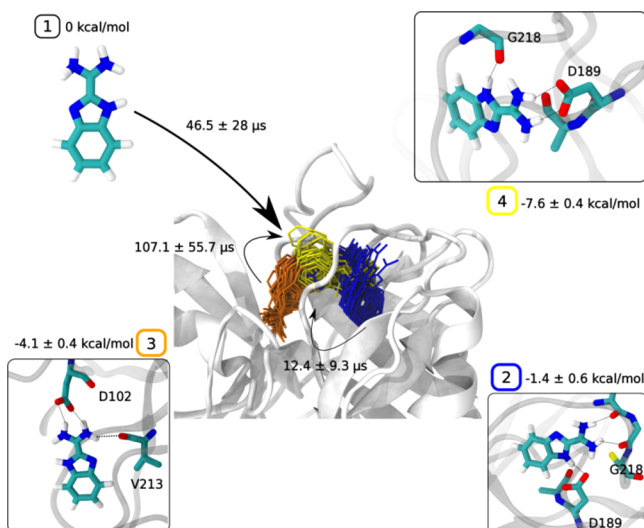
Figure 3. Example of an MSM analysis, fragment 31. MSM analysis computed four ligand-protein poses which can be visualized. One of the poses is the unbound state (state 1), and the other three are protein−ligand complexes stable at different extents. (Main poses are shown in the central figure.) For each pose, an estimate of relative free energy and mean first passage times to the other states can be computed. The analysis here presented was performed for the 42 fragments in this work.

energy difference between the unbound state (bulk) and the other states taking into account the fragment concentration in the simulation box (0.0037 M). As a result, the bound pose, located at the S1 pocket, possesses an affinity of −7.6 ± 0.4. Metastables poses 3 and 2 are −4.1 ± 0.4 and −1.4 ± 0.6 kcal/mol, respectively. The main transition to the bound pose occurs directly from the unbound state in 46.5 ± 28 μs, where it resides for a long time (12.1 ± 8.5 ms) interacting via H-bonds with Asp189. Transitions between bulk and poses 2 and 3 are also possible but occur in the millisecond time scale. Transitions among other states show metastable poses 2 and 3 revert to bound and unbound states in the microsecond time scale. The least stable pose 2 progresses to bound in 12.4 ± 9.3 μs and reverts to bulk in 7.0 ± 7.0 ms. From its side, metastable pose 3 moves to bound with slower kinetics, taking 107.1 ± 55.7 μs, and reverts to bulk in 382.2 ± 403.63 μs. The two metastable poses can also undergo transitions between them, although occurring in the millisecond time scale (106.5 ± 184 ms from pose 3 to pose 2 and 31.5 ± 24.6 ms for the inverse

process). A matrix showing all possible transitions is presented in Table S3.

If the k_{on} value is available experimentally, a simple way to estimate the computational cost is given by $t_{on} = C_{exp}/k_{on}$, where t_{on} would be the expected mean time to bind, and C_{exp} is the experimental concentration. For k_{off} estimation, note that it is not necessary to simulate for milliseconds in order to measure off-rates in the millisecond time scale. This is due to the fact that we are really computing transitions between states, and we are interested in accurate estimates of these transitions only in order to extrapolate the long-term, equilibrium behavior using the MSM theory. In the pathological case where we had only two states (bound and unbound), then it would be required to sample this event many times. However, we have usually thousands of states, which approximate the binding processing in many steps. Only the transitions between these steps must be sampled well. The fine grain of these transitions depends on both the metric projection used to transform the simulation data (e.g., contact maps, RMSD, contact distances) and the number of clusters used to discretize this space. In the optimal case where each hydrogen or salt bond formation can be distinguished then the simulation time should be just multiple times the time scale of the formation of a single pair interaction. Furthermore, new adaptive sampling schemes can substantially reduce the computational cost of more than 1 order of magnitude.[20]

Applying the analysis to the entire ligand set and ranking the free energy we find nine fragments with submillimolar affinity, as previously found by NMR experiments.[27] Their thermodynamic and their kinetic and thermodynamic data are shown in Table 1. Fragments 10, 27, 29, and 31 were expected to be among these hits,[27] and so occurred in our analysis except for the case of fragment 27. The precision in terms of affinity constants ranges from 10 to 48% relative to the mean, except for fragments 3 and 28 that showed greater dispersion (~100%). In terms of accuracy, fragment 29 (benzamidine) is remarkably accurate regarding the experimental value, with an estimated K_D of 85 ± 12 versus the reported 80 μM. Fragments 10 and 31 failed to reproduce the experimental value within one standard deviation, although both are found in the same micromolar range and succeeded in reproducing the relative ranking. Fragments 36 and 37 also had annotated values,[28] being the latter's experimental value within our standard deviation (−1.8 ± 0.8 versus the experimental −2.6 kcal/mol). Fragment 36 did not agree well with experimental findings (ΔG_{exp} = −5.8 versus −2.5 kcal/mol), probably due to the shortcoming of the force field in resolving halogen bonds.[37]

Table 1. Table Showing Our Quantitative Results for Kinetic (k_{on}, k_{off}) and Thermodynamic Data (K_D, ΔG^0, and Experimental K_D When Available)[a]

Pos.	ID	ΔG° (kcal/mol)	k_{off} (s^{-1})	k_{on} (s^{-1} M^{-1})	$k_{D,calc}$ (μM)	$k_{D,exp}$ (μM)
1	31	−7.6 ± 0.4	(1.1 ± 0.6) × 10^2	(8.0 ± 4.8) × 10^6	3.1 ± 1.5	30
2	29	−5.6 ± 0.1	(1.1 ± 0.2) × 10^4	(1.1 ± 0.2) × 10^8	85 ± 12	80
3	18	−5.6 ± 0.2	(3.7 ± 1.0) × 10^3	(2.9 ± 0.4) × 10^7	75 ± 17	
4	21	−5.5 ± 0.5	(1.1 ± 1.3) × 10^4	(6.8 ± 1.8) × 10^7	130 ± 14	
5	28	−5.0 ± 0.5	(1.6 ± 1.8) × 10^4	(5.2 ± 0.4) × 10^7	290 ± 340	
6	13	−4.4 ± 0.3	(1.2 ± 0.5) × 10^5	(1.8 ± 0.2) × 10^8	630 ± 240	
7	12	−4.1 ± 0.3	(9.6 ± 3.6) × 10^4	(7.8 ± 1.3) × 10^7	1200 ± 580	
8	10	−4.0 ± 0.2	(2.1 ± 0.2) × 10^4	(1.2 ± 0.3) × 10^7	1300 ± 470	210
9	3	−4.0 ± 0.6	(7.3 ± 6.1) × 10^4	(3.7 ± 1.0) × 10^7	1700 ± 1700	

[a]The 9 submillimolar fragments in the topmost positions (Pos.) in the ranking of the library, and their annotated affinities when available are shown.

Additionally, fragment 15, had been part of a kinetic study with bovine trypsin[38] in which it showed an IC_{50} in mM range, compared to low μM for benzamidine. The same trend and similar affinity are present in our analysis ($K_D = 3.6 \pm 3.1$ mM).

Next, we shifted our attention toward understanding the molecular determinants that define binding kinetics. All molecules are fast binders, showing in the slowest case (fragment 31) on and off-rates of the order of 10^6 M^{-1} s^{-1} and 10^2 s^{-1}, respectively (Table 1). Benzamidine's (29) binding kinetics to trypsin protease have been studied in the past,[39] with on-rate $2.9 \pm \cdot 10^7$ $M^{-1}\cdot s^{-1}$ and off-rates $6.0 \pm \cdot 10^2$ s^{-1}. Our on-rate for factor Xa is in the low 10^8 M^{-1} s^{-1} time scale. The off-rate, however, is 2 orders of magnitude faster, compatible with the lower affinity of benzamidine for factor Xa relative to trypsin.[40] In terms of the entire library, molecular properties such as molecular weight, number of rotatable bonds, charge, and lipophilicity did not provide any significant statistical correlation with either kinetic parameter. However, a closer inspection into the kinetic rate plot (Figure 4) revealed
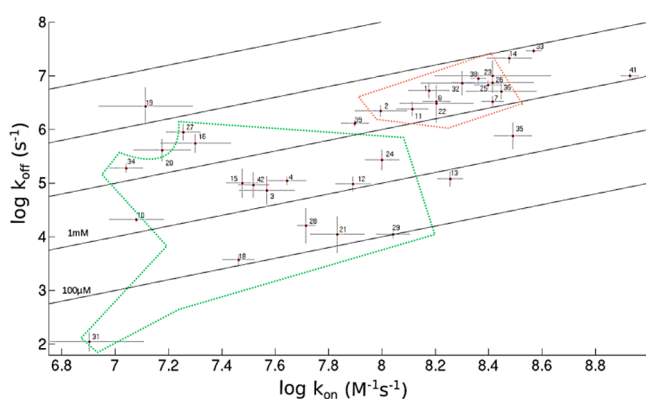

Figure 4. Interaction rate plot for a set of 35 fragments. The x and y axes represent the on and off-rates. Crosswise lines represent affinities (K_D). The slowest and more resident binders - showing the strongest affinities - are all S1 binders containing amide or amidine moieties (encircled in green). All the neutral S1 binders except 42 showed moderated unbinding and binding times (encircled in orange).

that, for this particular protease, ligands could be divided into two groups. Basic amidine or amine S1-binders displayed the slowest on and off rates (green), while all neutral S1 binders showed intermediate on and off rates (orange).

Regarding the most probable binding modes, 15 of the fragments were experimentally known to bind at the S1 pocket (Figure 2, **superscript a**). The primary binding poses and their correlation with the crystallographic pose for a set of examples is shown in Figure 5 (entire set of primary poses is shown in the html table in the Supporting Information). From the 15 S1 binders, five are identically available in X-ray structures, specifically, fragments 19 (benzylamine), 15 (histamine), 24 (2-aminopyridine), 35, and benzamidine (29), all known protease ligands forming hydrogen bonds with Asp189, where the first four have been used as less-basic benzamidine mimics.[41] Three of them also showed their bound pose in the S1 preserving the X-ray contacts (Figure 5, **first row.**) Another six of these fragments have been used as S1-moieties in larger bioactive factor Xa inhibitors (fragments 6, 8, 18, 26, 36 and 38). In detail, fragments 6, 8, and 26 are indole and its 6-position hydroxyl, and amine-derivatives a moiety widely found as a S1 substituent in many inhibitors. Fragment 8 showed a
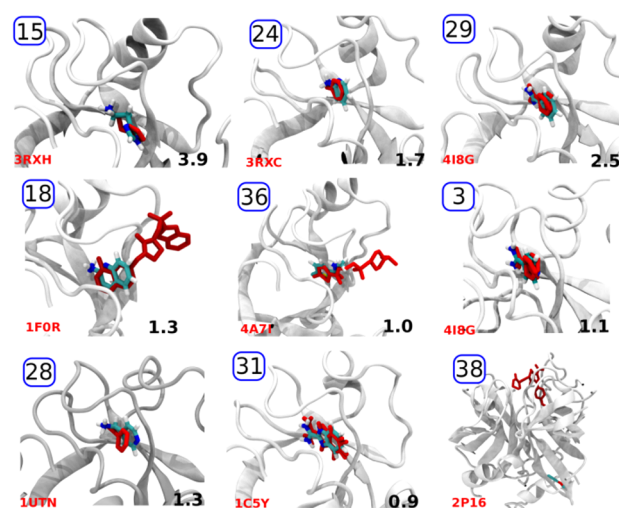

Figure 5. Comparison between the average pose of our primary bound state (in cyan) and the available X-ray pose (in red) for the fragments with expected S1 poses. Fragment ID is shown in black, while the respective PDB code for each of the structures is shown in red. Each picture is accompanied by the average RMSD of the state to the reference crystal. All fragments show accurate superimposition except the case of fragment 38 in which the bound pose was found at a pocket different than the expected S1.

defined first pose in the S1 pocket. Fragments 6 and 26 did not bind in their first pose to the S1 pocket but did in the secondary poses.

Fragment 18, aminoisoquinoline, has been exploited as a benzamidine bioisoster in many projects, and the analysis gave a defined pose in agreement with X-ray data (RMSD 1.2 Å). Fragment 36 (chlorothiophene) was found to occupy the S1 site targeted by a new generation of bioavailable neutral inhibitors. It is also present in the oral anticoagulant rivaroxaban and presented a pose very similar to the experimental one (RMSD 1.0 Å). In contrast, our analysis failed to recover the expected primary pose in the S1 pocket for ligand 38 (anisole, in apixaban inhibitor), yielding only a low-affinity pose. Fragments 3 (4-amidinopyridine) and 12 are structurally similar to cocrystallized fragments in trypsin, and both recovered the X-ray structures. The RMSD for all S1 expected binders is presented in Table S2.

Interestingly, the results for the ten expected S4 binders presented a very different scenario. Poses found in the S4 pocket were generally less defined with lower residence times and had lower affinity than those in the S1 analogue. Specifically, only 2 out of the 42 fragments showed their most probable pose within the S4 cavity. In the case of the set of ten expected S4-binders (Figure 2), only fragment 4 showed their first binding pose within the S4 pocket; all the others except fragment 37 showed preferential binding to the S1 pocket. Interestingly, a recent factor Xa inhibitors deconstruction experiment, which included fragment 37, showed that S4 fragments did not significantly bind or inhibit factor Xa.[36] It is thus important to stress that a prototypical fragment screening approach would have been unlikely to identify the potential of these fragments as S4 molecules.

Furthermore, we observed the flipping of Trp215 toward the catalytic triad and opening of a wider and otherwise inaccessible S4 pocket in some simulations where fragments formed metastable S4 poses (Supporting Figure S1a). To further test this alternative S4 conformation and corresponding new

pocket, we performed a conformational study of the *apo*-protein with a different force field (Supporting Information, **Methods**) to assess whether this novel conformation was a simulation artifact. We produced 850 simulations of 30 ns each giving a total aggregate of 26 μs. A simple analysis of this simulation batch showed notable mobility of Trp215 between the crystal pose and the new pose and of the loop between residues 215−225 of the protein. The conformation with Trp215 flipped toward S1 is sampled by both force fields. A further literature search yielded experimental evidence that a similar allosteric transition had been observed in the related protease thrombin, where Trp215 acts as an S1 pocket gatekeeper, moving 10.6 Å in the process[42,43] (Figure S1). Additionally, kinetic measurements had previously demonstrated the same phenomenon could occur in factor Xa,[44] on the millisecond time scale.

CONCLUSION

In conclusion, we have presented the simultaneous determination of fragment binding poses, thermodynamics, and kinetics to augment and understand experimental fragment-hit identification screening data. Comparisons with affinity data showed good agreement in four out of the six cases that have experimental K_D. The binding modes of expected S1-pocket binders overlapped well with available crystal structures in all but three of the 15 cases. For the case of known S4 moieties, only one of the fragments found the primary pose predicted from its location in larger lead-like compounds. We also provide valuable additional insight on the specific binding kinetic characteristics of the protein cavities, existence of possible allosteric sites, and guidelines on the specific role that each moiety will adopt in larger inhibitors. In the specific case of this protease, the S1 subpocket is the major driver of binding, with around 60% of the fragments binding preferentially within it. Furthermore, the identification of metastable binding poses for many of the fragments screened offers unique and highly relevant information for follow-up fragment growth and linking strategies. For instance, a partially positively charged para-substituted benzamidine bound at the S1 pocket could stabilize the opening of the S4 pocket, by interacting favorably with Trp215. In this respect, the *in silico* method presented here complements well existing experimental data.

The significant computational cost of the sampling required for this type of study currently limits its application beyond focused fragment libraries with fast kinetics. However, the continuous increase of computational power, as well as the development of new sampling schemes,[20] will certainly make these calculations standard in the not so distant future.

ASSOCIATED CONTENT

⑤ Supporting Information

The Supporting Information is available free of charge on the ACS Publications website at DOI: 10.1021/acs.jcim.5b00453.

　Methods, Tables S1−S3, and Figure S1 (PDF)
　Set of entire results as a webdata html table (ZIP)

AUTHOR INFORMATION

Corresponding Author
*E-mail: gianni.defabritiis@upf.edu.
Notes
The authors declare no competing financial interest.

REFERENCES

(1) Shuker, S. B.; Hajduk, P. J.; Meadows, R. P.; Fesik, S. W. Discovering High-Affinity Ligands for Proteins: SAR by NMR. *Science* **1996**, *274*, 1531−1534.

(2) Warr, W. A. Fragment-Based Drug Discovery. *J. Comput.-Aided Mol. Des.* **2009**, *23*, 453−458.

(3) Erlanson, D. A. Introduction to Fragment-Based Drug Discovery. *Top. Curr. Chem.* **2011**, *317*, 1−32.

(4) Murray, C. W.; Verdonk, M. L.; Rees, D. C. Experiences in Fragment-Based Drug Discovery. *Trends Pharmacol. Sci.* **2012**, *33*, 224−232.

(5) Davis, B. J.; Erlanson, D. A. Learning from Our Mistakes: The "Unknown Knowns" in Fragment Screening. *Bioorg. Med. Chem. Lett.* **2013**, *23*, 2844−2852.

(6) Mashalidis, E. H.; Śledź, P.; Lang, S.; Abell, C. A Three-Stage Biophysical Screening Cascade for Fragment-Based Drug Discovery. *Nat. Protoc.* **2013**, *8*, 2309−2324.

(7) Dolezal, O.; Doughty, L.; Hattarki, M. K.; Fazio, V. J.; Caradoc-Davies, T. T.; Newman, J.; Peat, T. S. Fragment Screening for the Modelling Community: SPR, ITC, and Crystallography. *Aust. J. Chem.* **2013**, *66*, 1507−1517.

(8) Talele, T. T.; Khedkar, S. A.; Rigby, A. C. Successful Applications of Computer Aided Drug Discovery: Moving Drugs from Concept to the Clinic. *Curr. Top. Med. Chem.* **2010**, *10*, 127−141.

(9) Verdonk, M. L.; Giangreco, I.; Hall, R. J.; Korb, O.; Mortenson, P. N.; Murray, C. W. Docking Performance of Fragments and Druglike Compounds. *J. Med. Chem.* **2011**, *54*, 5422−5431.

(10) Leach, A. R.; Shoichet, B. K.; Peishoff, C. E. Prediction of Protein-Ligand Interactions. Docking and Scoring: Successes and Gaps. *J. Med. Chem.* **2006**, *49*, 5851−5855.

(11) Shan, Y.; Kim, E. T.; Eastwood, M. P.; Dror, R. O.; Seeliger, M. A.; Shaw, D. E. How Does a Drug Molecule Find Its Target Binding Site? *J. Am. Chem. Soc.* **2011**, *133*, 9181−9183.

(12) Bisignano, P.; Doerr, S.; Harvey, M. J.; Favia, A. D.; Cavalli, A.; De Fabritiis, G. Kinetic Characterization of Fragment Binding in AmpC β-Lactamase by High-Throughput Molecular Simulations. *J. Chem. Inf. Model.* **2014**, *54*, 362−366.

(13) Yu, W.; Lakkaraju, S. K.; Raman, E. P.; Fang, L.; MacKerell, A. D. Pharmacophore Modeling Using Site-Identification by Ligand Competitive Saturation (SILCS) with Multiple Probe Molecules. *J. Chem. Inf. Model.* **2015**, *55*, 407−420.

(14) Schmidtke, P.; Barril, X. Understanding and Predicting Druggability. A High-Throughput Method for Detection of Drug Binding Sites. *J. Med. Chem.* **2010**, *53*, 5858−5867.

(15) Alvarez-Garcia, D.; Barril, X. Molecular Simulations with Solvent Competition Quantify Water Displaceability and Provide Accurate Interaction Maps of Protein Binding Sites. *J. Med. Chem.* **2014**, *57*, 8530−8539.

(16) Sadiq, S. K.; Noé, F.; De Fabritiis, G. Kinetic Characterization of the Critical Step in HIV-1 Protease Maturation. *Proc. Natl. Acad. Sci. U. S. A.* **2012**, *109*, 20449.

(17) Bowman, G. R.; Huang, X.; Pande, V. S. Using Generalized Ensemble Simulations and Markov State Models to Identify Conformational States. *Methods* **2009**, *49*, 197−201.

(18) Noé, F.; Fischer, S. Transition Networks for Modeling the Kinetics of Conformational Change in Macromolecules. *Curr. Opin. Struct. Biol.* **2008**, *18*, 154−162.

(19) Buch, I.; Giorgino, T.; De Fabritiis, G. Complete Reconstruction of an Enzyme-Inhibitor Binding Process by Molecular Dynamics Simulations. *Proc. Natl. Acad. Sci. U. S. A.* **2011**, *108*, 10184−10189.

(20) Doerr, S.; De Fabritiis, G. On-the-Fly Learning and Sampling of Ligand Binding by High-Throughput Molecular Simulations. *J. Chem. Theory Comput.* **2014**, *10*, 2064.

(21) Bowman, G. R.; Ensign, D. L.; Pande, V. S. Enhanced Modeling via Network Theory: Adaptive Sampling of Markov State Models. *J. Chem. Theory Comput.* **2010**, *6*, 787−794.

(22) Lawrenz, M.; Shukla, D.; Pande, V. S. Cloud Computing Approaches for Prediction of Ligand Binding Poses and Pathways. *Sci. Rep.* **2015**, *5*, 7918.

(23) Huang, D.; Caflisch, A. The Free Energy Landscape of Small Molecule Unbinding. *PLoS Comput. Biol.* **2011**, *7*, e1002002.

(24) Pinto, D. J. P.; Smallheer, J. M.; Cheney, D. L.; Knabb, R. M.; Wexler, R. R. Factor Xa Inhibitors: Next-Generation Antithrombotic Agents. *J. Med. Chem.* **2010**, *53*, 6243−6274.

(25) Lin, Z.; Johnson, M. E. Proposed Cation-π Mediated Binding by Factor Xa: A Novel Enzymatic Mechanism for Molecular Recognition. *FEBS Lett.* **1995**, *370*, 1−5.

(26) Brandstetter, H.; Kühne, A.; Bode, W.; Huber, R.; von der Saal, W.; Wirthensohn, K.; Engh, R. A. X-Ray Structure of Active Site-Inhibited Clotting Factor Xa. Implications for Drug Design and Substrate Recognition. *J. Biol. Chem.* **1996**, *271*, 29988−29992.

(27) Fielding, L.; Fletcher, D.; Rutherford, S.; Kaur, J.; Mestres, J. Exploring the Active Site of Human Factor Xa Protein by NMR Screening of Small Molecule Probes. *Org. Biomol. Chem.* **2003**, *1*, 4235−4241.

(28) Maignan, S.; Guilloteau, J. P.; Pouzieux, S.; Choi-Sledeski, Y. M.; Becker, M. R.; Klein, S. I.; Ewing, W. R.; Pauls, H. W.; Spada, A. P.; Mikol, V. Crystal Structures of Human Factor Xa Complexed with Potent Inhibitors. *J. Med. Chem.* **2000**, *43*, 3226−3232.

(29) Lee, Y.-K.; Parks, D. J.; Lu, T.; Thieu, T. V.; Markotan, T.; Pan, W.; McComsey, D. F.; Milkiewicz, K. L.; Crysler, C. S.; Ninan, N.; Abad, M. C.; Giardino, E. C.; Maryanoff, B. E.; Damiano, B. P.; Player, M. R. 7-Fluoroindazoles as Potent and Selective Inhibitors of Factor Xa†. *J. Med. Chem.* **2008**, *51*, 282−297.

(30) Harvey, M. J.; Giupponi, G.; De Fabritiis, G ACEMD: Accelerating Biomolecular Dynamics in the Microsecond Time Scale. *J. Chem. Theory Comput.* **2009**, *5*, 1632−1639.

(31) Buch, I.; Harvey, M. J.; Giorgino, T.; Anderson, D. P.; De Fabritiis, G. High-Throughput All-Atom Molecular Dynamics Simulations Using Distributed Computing. *J. Chem. Inf. Model.* **2010**, *50*, 397.

(32) www.htmd.org www.htmd.org (accessed Sept 1, 2015).

(33) Held, M.; Noé, F. Calculating Kinetics and Pathways of Protein−ligand Association. *Eur. J. Cell Biol.* **2012**, *91*, 357−364.

(34) Voelz, V. A.; Bowman, G. R.; Beauchamp, K.; Pande, V. S. Molecular Simulation of Ab Initio Protein Folding for a Millisecond Folder NTL9(1−39). *J. Am. Chem. Soc.* **2010**, *132*, 1526−1528.

(35) Stanley, N.; Esteban-Martín, S.; De Fabritiis, G. Kinetic Modulation of a Disordered Protein Domain by Phosphorylation. *Nat. Commun.* **2014**, *5*, 5272.

(36) Nazaré, M.; Matter, H.; Will, D. W.; Wagner, M.; Urmann, M.; Czech, J.; Schreuder, H.; Bauer, A.; Ritter, K.; Wehner, V. Fragment Deconstruction of Small, Potent Factor Xa Inhibitors: Exploring the Superadditivity Energetics of Fragment Linking in Protein−Ligand Complexes. *Angew. Chem., Int. Ed.* **2012**, *51*, 905−911.

(37) Ibrahim, M. A. A. Molecular Mechanical Study of Halogen Bonding in Drug Discovery. *J. Comput. Chem.* **2011**, *32*, 2564−2574.

(38) Yamane, J.; Yao, M.; Zhou, Y.; Hiramatsu, Y.; Fujiwara, K.; Yamaguchi, T.; Yamaguchi, H.; Togame, H.; Tsujishita, H.; Takemoto, H.; Tanaka, I. In-Crystal Affinity Ranking of Fragment Hit Compounds Reveals a Relationship with Their Inhibitory Activities. *J. Appl. Crystallogr.* **2011**, *44*, 798−804.

(39) Guillain, F.; Thusius, D. Use of Proflavine as an Indicator in Temperature-Jump Studies of the Binding of a Competitive Inhibitor to Trypsin. *J. Am. Chem. Soc.* **1970**, *92*, 5534−5536.

(40) Katz, B. A.; Mackman, R.; Luong, C.; Radika, K.; Martelli, A.; Sprengeler, P. A.; Wang, J.; Chan, H.; Wong, L. Structural Basis for Selectivity of a Small Molecule, S1-Binding, Submicromolar Inhibitor of Urokinase-Type Plasminogen Activator. *Chem. Biol.* **2000**, *7*, 299−312.

(41) Lam, P. Y. S.; Clark, C. G.; Li, R.; Pinto, D. J. P.; Orwat, M. J.; Galemmo, R. A.; Fevig, J. M.; Teleha, C. A.; Alexander, R. S.; Smallwood, A. M.; Rossi, K. A.; Wright, M. R.; Bai, S. A.; He, K.; Luettgen, J. M.; Wong, P. C.; Knabb, R. M.; Wexler, R. R. Structure-Based Design of Novel Guanidine/benzamidine Mimics: Potent and Orally Bioavailable Factor Xa Inhibitors as Novel Anticoagulants. *J. Med. Chem.* **2003**, *46*, 4405−4418.

(42) Niu, W.; Chen, Z.; Gandhi, P. S.; Vogt, A. D.; Pozzi, N.; Pelc, L. A.; Zapata, F.; Di Cera, E. Crystallographic and Kinetic Evidence of Allostery in a Trypsin-like Protease. *Biochemistry* **2011**, *50*, 6301−6307.

(43) Niu, W.; Chen, Z.; Bush-Pelc, L. A.; Bah, A.; Gandhi, P. S.; Di Cera, E. Mutant N143P Reveals How Na+ Activates Thrombin. *J. Biol. Chem.* **2009**, *284*, 36175−36185.

(44) Vogt, A. D.; Bah, A.; Di Cera, E. Evidence of the E*-E Equilibrium from Rapid Kinetics of Na+ Binding to Activated Protein C and Factor Xa*. *J. Phys. Chem. B* **2010**, *114*, 16125−16130.